

Cite as: Phys. Fluids **34**, 032006 (2022); https://doi.org/10.1063/5.0085967 Submitted: 20 January 2022 • Accepted: 21 February 2022 • Published Online: 07 March 2022

🗓 Michael Dacus, 🗓 Mahmud Kamal Raihan, Micah Baghdady, et al.

COLLECTIONS

F This paper was selected as an Editor's Pick







ew Online Export C





Cite as: Phys. Fluids **34**, 032006 (2022); doi: 10.1063/5.0085967 Submitted: 20 January 2022 · Accepted: 21 February 2022 · Published Online: 7 March 2022







AFFILIATIONS

- ¹Department of Mechanical Engineering, Clemson University, Clemson, South Carolina 29634-0921, USA
- ²College of Marine Engineering, Dalian Maritime University, Dalian 116026, China

ABSTRACT

Surfactants are often added to particle suspensions in the flow of Newtonian or non-Newtonian fluids for the purpose of reducing particle-particle aggregation and particle-wall adhesion. However, the impact on the flow behavior of such surfactant additions is often overlooked. We experimentally investigate the effect of the addition of a frequently used neutral surfactant, Tween 20, at the concentration pertaining to microfluidic applications on the entry flow of water and three common polymer solutions through a planar cavity microchannel. We find that the addition of Tween 20 has no significant influence on the shear viscosity or extensional flow of Newtonian water and Boger polyethylene oxide solution. However, such a surfactant addition reduces both the shear viscosity and shear-thinning behavior of xanthan gum and polyacrylamide solutions that each exhibit a strong shear-thinning effect. It also stabilizes the cavity flow and delays the onset of flow instability in both cases. The findings of this work can directly benefit microfluidic applications of particle and cell manipulation in Newtonian and non-Newtonian fluids.

Published under an exclusive license by AIP Publishing. https://doi.org/10.1063/5.0085967

I. INTRODUCTION

Polymer solutions are frequently encountered in the fields of biomedical engineering, petroleum science, cosmetics, and food processing.¹⁻³ Surfactant compounds are widely used in solutions to stabilize emulsions and foams, enhance cleaning and wetting, and facilitate dispersing in industries, such as painting, coating, and pharmaceuticals.^{4,5} They usually have a hydrophilic body and a hydrophobic tail, which seek out the interfaces between aqueous and nonaqueous layers and deposit therein reducing the interfacial tension. They can be either ionic, nonionic, or neutrally charged in nature. In microfluidics specifically, surfactants are frequently added to control droplet sizes and shapes. 6-8 They are also often added to particle suspensions prepared in either Newtonian^{9–12} or non-Newtonian^{13–17} fluids for the purpose of reducing both particle-wall adhesion and particle-particle aggregation. Despite this relevance, however, the rheological impact on microfluidic flows and particle motion due to the presence of surfactant has been largely ignored.

The role of surfactants in solutions has been the focus of numerous studies. Del Sorbo *et al.*¹⁸ reported that the shear thinning in the oppositely charged polyelectrolyte and sodium dodecyl sulfate (SDS) surfactant system is related to the rupture of the mixed rodlike

aggregates in which the surfactant cross-links several polyelectrolyte chains. Ye et al. 19 found that ionic, nonionic, and zwitterionic surfactants all have the similar effect of enhancing the shear-thickening behavior of the condensed polymer nanosphere dispersions. Bollineni et al.²⁰ investigated the complex interactions among the ions present in solutions of nanoparticles, surfactants, and electrolytes (NSE). They found that the viscosity profile of NSE solutions with the increasing concentration of SDS surfactant behaves like spherical particles. Xu et al.²¹ studied the effects of surfactant type and concentration on the size of droplet formation, where a higher-concentration surfactant was found necessary in the formation of smaller droplets. Yang and Pal²² studied the interactions between a drag-reducing polymer and five different surfactants. The critical aggregation concentration of surfactants was found to depend on the ionic charges of both the polymer and surfactant. Martínez Narvaez et al.²³ reported that the polyethylene oxide (PEO) and SDS mixtures display a significantly weaker concentrationdependent variation in the extensional relaxation time and viscosity than anticipated by the measured shear viscosity. Ahmadikhamsi et al.²⁴ studied the viscous fingering in the displacement of an oil phase by a non-Newtonian fluid with and without SDS addition. They found that the relative finger widths in both experiments converge

^{a)}Authors to whom correspondence should be addressed: xcxuan@clemson.edu and yongxin@dlmu.edu.cn

asymptotically to the same value because of the decreased surfactant concentration in the vicinity of the tip of growing finger.

Most of the previous studies concern surfactant solutions of moderately high concentrations, which highlight the effects of surfactant concentration and charge as well as the ionic charge of the polymer on fluid rheology. However, rheological alterations with smaller surfactant concentrations on the order of 0.1% v/v, which is commonly used in microfluidic devices, 9-16 have received comparably less attention. Even less understood is the impact of surfactant addition on the flow behavior. We investigate in this work the effect of the addition of 0.5% v/v Tween 20 on the shear viscosity and extensional flow response of three common polymer solutions in microfluidic applications, namely, xanthan gum (XG), PEO, and polyacrylamide (PAA) solutions along with the Newtonian de-ionized (DI) water. 25-29 To the best of our knowledge, this work is the first study on the topic and will advance the understanding of surfactant addition on fluid flow and particle motion in microfluidic devices. We seed microparticles into each of these solutions both with and without the surfactant for visualization and direct comparison of the flow patterns through a cavity microchannel with a single expansion-contraction structure. Contraction and/or expansion channels are commonly occurring structures in microfluidic applications. 30-34 They have been employed for particle focusing, trapping, and sorting purposes in both Newtonian^{35–39} Newtonian 40-44 fluids, where surfactants are necessary to de-cluster particles for stable performance. Such channels are also the benchmark structures for the characterization of non-Newtonian fluids, in which elastic instabilities can emerge at low Reynolds numbers due to flow extension and thus be isolated from the fluid inertial effect. 45-50 The rest of this paper is organized as follows: Sec. II describes the experimental setup. Section III presents and discusses the extensional flows of Newtonian and non-Newtonian fluids both with and without the addition of Tween 20. Section IV summarizes the findings of this work and outlines some potential future work.

II. EXPERIMENT

A. Materials

Figure 1 shows a photo of the cavity microchannel used for the tests. The channel mold was fabricated by conventional

photolithography with SU-8 25 (MicroChem, Newton, MA, USA). The microchannel was then prepared from the mold by soft lithography with polydimethylsiloxane (PDMS). The detailed steps of the preparation procedure can be found in our previous work.⁵¹ The channel is overall 2 cm long including the inlet and outlet reservoirs. It has a single expansion-contraction at the center with a length and width of about 500 μ m each. The width of the main channel is 50 μ m and the depth is uniformly 45 μ m. Four different solutions were used in our tests: Newtonian DI water (Fisher Scientific, Waltham, MA, USA), viscoelastic PEO solution (1000 ppm, $M_w = 2$ MDa, Sigma-Aldrich, St Louis, MO, USA) with negligible shear thinning (i.e., Boger fluid⁵²), shear-thinning XG solution (1000 ppm, molecular weight, $M_w \approx 2$ MDa, Tokyo Chemical Industry, Tokyo, Japan) with negligible elasticity, and both viscoelastic and shear thinning PAA solution (200 ppm, $M_w = 18$ MDa, Polysciences, Warrington, PA, USA). All the polymer solutions used here are in their respective semi-dilute conformation regimes.⁵³ To test the effect of surfactant, Tween 20 (0.5% v/v, Fisher Scientific, Waltham, MA, USA) was added to each of the prepared solutions. It is a neutrally charged polymer,⁵⁴ which minimizes the effect of ionic interaction and emphasizes on the rheological change as the main focus of this work.

Figure 2 shows the viscosities of the prepared solutions with and without Tween 20 that were measured using a cone-plate rheometer (Anton Paar, MCR 302) for shear rate spanning from 0.1 to 10 000 s⁻¹ at room temperature. We find that the addition of 0.5% v/v Tween 20 significantly suppresses the shear thinning effect of the XG and PAA solutions. It, however, appears to have a negligible impact on the (nearly) constant viscosity profile of the water and PEO solution. We used the Carreau model⁵⁵ to fit the measured viscosity data for the solutions exhibiting visible shear thinning effects (see the fitting lines in Fig. 2),

$$\frac{\eta - \eta_{\infty}}{\eta_0 - \eta_{\infty}} = \left[1 + (\lambda_c \dot{\gamma})^2\right]^{(n-1)/2},\tag{1}$$

where η_{∞} is the infinite-shear-rate viscosity, η_0 is the zero shear-rate viscosity, λ_c is a time constant, $\dot{\gamma}$ is the fluid shear rate, and n is the power-law index. We also attempted to measure the relaxation times, λ , of the polymer solutions, but failed to obtain consistent and accurate



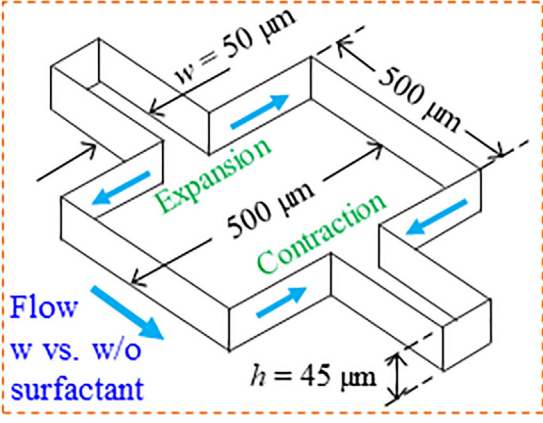


FIG. 1. Isometric view of the prepared cavity microchannel (left) and schematic illustration of the expansion—contraction part (highlighted by the dashed box, left) with respective dimensions (right).

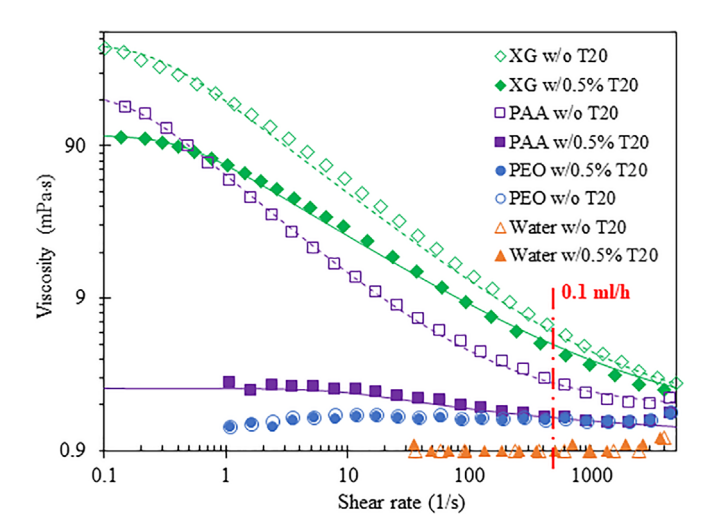


FIG. 2. Experimentally measured (symbols) and theoretically fitted (lines, via the Carreau model) viscosity data of the prepared solutions. The vertical dashed-dotted line indicates the shear rate in the main channel for the flow rate of 0.1 ml/h.

data using our rheometer. We thus decided to employ the reported experimental values in the literature that used exactly the same solutions as in this work. ^{56–58} Moreover, as no apparent difference is viewed from the flow pattern of water or PEO solution (see Sec. III), we hypothesize here that the addition of small amount of Tween 20 does not affect the fluid elasticity. The relaxation times and the fitting parameters in the Carreau model for the prepared solutions are listed in Table I.

B. Methods

The flow in the expansion–contraction region of the cavity microchannel was visualized by seeding 1 μ m diameter fluorescent particles (Bangs Laboratories, Fishers, IN, USA) into each of the prepared solutions at the concentration of the order of 0.01% v/v. The influences of these particles on the fluid rheology and flow behavior are neglected in this work considering the low concentration. The

TABLE I. Summary of the fitting parameters in the Carreau model for the experimentally measured viscosity data along with the relaxation times of the prepared solutions with and without 0.5% v/v Tween 20 addition.

Solution	n	η_0 (mPa s)	η_{∞} (mPa s)	λ_C (ms)	λ (ms)
DI water	1	0.9			0
DI water w/0.5%	1	0.9			$\sim \! 0$
XG	0.38	420	1.6	4	$\sim \! 0^{\mathrm{a}}$
XG w/0.5%	0.50	105	1.35	2.3	~ 0
PEO	~ 1	1.5			1.5 ^b
PEO w/0.5%	~ 1	1.5			~ 1.5
PAA	0.30	160	1.7	3.8	95°
PAA w/0.5%	0.72	2.3	1.1	0.08	\sim 95

aHaase et al.56

particle suspension was driven through the channel with a syringe pump (KD Scientific, Holliston, MA, USA) that was connected to the inlet reservoir via a plastic tube. Another plastic tube was inserted into the outlet reservoir that led the fluid out of the channel to a vial. The motion of the seeded particles was recorded through an inverted fluorescent microscope (Nikon Eclipse TE2000U, Nikon Instruments) with a CCD camera (Nikon DS-Qi1Mc). The exposure time of the camera for the captured snapshots ranged between 0.5 and 3 s. For higher flow rates, it was set at lower values in the range to adapt to the faster movement of the tracer particles. The obtained images were post-processed using the Nikon imaging software (NIS Elements AR 3.22).

The inertial effect on the cavity flow of fluids with or without Tween 20 is studied in terms of the (channel) Reynolds number,

$$Re = \frac{\rho V D_h}{\eta(\overline{\dot{\gamma}})} = \frac{2\rho Q}{\eta(\overline{\dot{\gamma}})(w+h)},$$
 (2)

where ρ is the mass density (assumed equal to that of the suspending water), V is the average fluid velocity in the main channel, D_h is the hydraulic diameter of the main channel, $\eta(\overline{\gamma})$ is the fluid viscosity at the average shear rate, $\overline{\gamma}=2V/w$, across the width, $w=50~\mu\text{m}$, of the main channel, Q is the volumetric flow rate, and $h=45~\mu\text{m}$ is the channel height. The flow rate, Q, in our experiment is varied from about 0.1–40 ml/h, for which the calculated shear rate, $\overline{\gamma}$, ranges between 494 1/s (as highlighted by the vertical dashed-dotted line in Fig. 2) and 1.975×10^5 1/s. The fluid elasticity effect on the flow is characterized by the Weissenberg number,

$$Wi = \lambda \overline{\dot{\gamma}} = \frac{2\lambda Q}{w^2 h}.$$
 (3)

The fluid shear thinning effect is compared in terms of the power-law index, n, in the Carreau model (see Table I). For the ease of reference, we consider a fluid to be strongly shear thinning if n < 0.65 as suggested by Lindner *et al.*⁵⁹

III. RESULTS AND DISCUSSION

A. Newtonian water

Figure 3 compares the inertial flows of water with and without the addition of 0.5% Tween 20 through the expansion-contraction part of the microchannel. The measured viscosities in Fig. 2 indicate that there are barely any changes between the two fluids for the range of shear rates tested. Figure 3 demonstrates that there is hardly any difference in the flow development for water with and without surfactant. In both cases, the streamlines remain undisturbed for flow rates of up to 4 ml/h (Re = 26.0). A flow separation occurs at the expansion walls in the form of lip vortices at around 5 ml/h (Re = 32.5). These inertially formed vortices grow on to reach the salient corners of the cavity at around 9 ml/h (Re = 58.5). With the further increase in the flow rate, the corner vortices extend only in the flow direction and reach the contraction walls at around 15 ml/h (Re = 97.5). They occupy almost half of the cavity at 19 ml/h (Re = 123.5). During this process, the vortices remain symmetric and steady in both solutions, indicating an insignificant elasticity effect brought by the addition of Tween 20 or at least negligible as compared to the inertial effect.

Figure 4 shows the measured vortex size along the length, L_{ν} (see the highlighted dimension in Fig. 3, normalized by the length of the cavity), against Re in the expansion flow of water with and without

^bRodd et al.⁵⁷

^cPoole and Escudier.⁵⁸

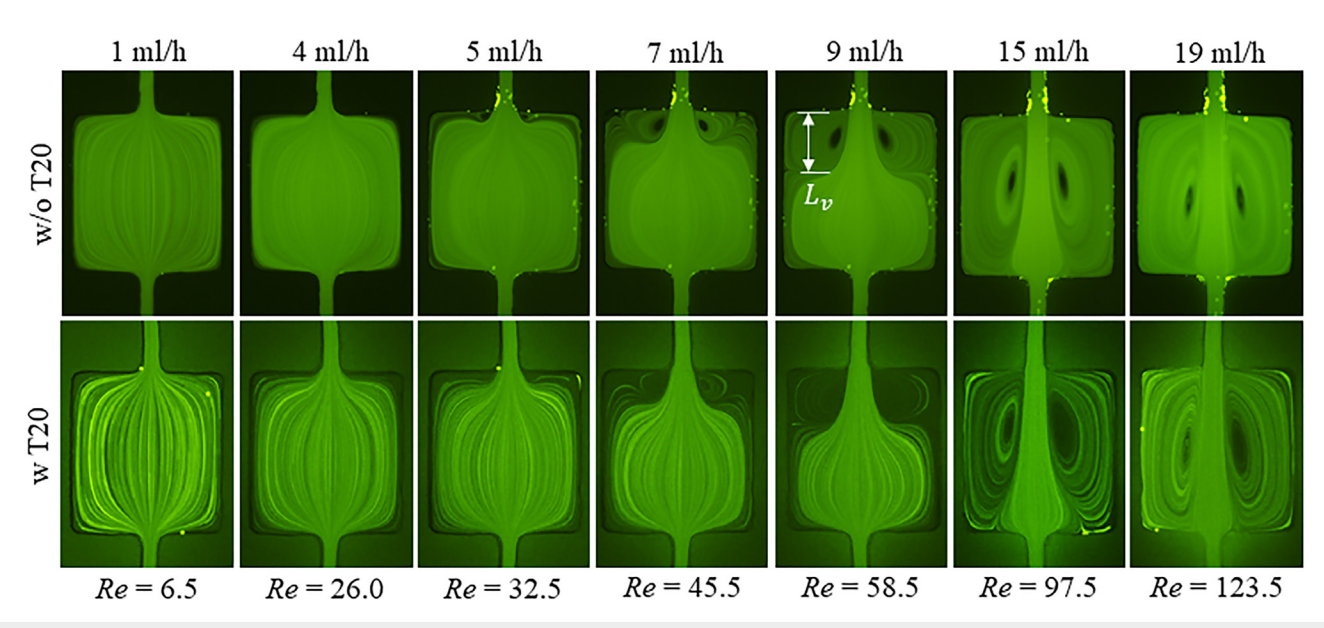


FIG. 3. Snapshot images of the flow of Newtonian water without (w/o T20, top row) and with (w T20, bottom row) 0.5% Tween 20 through the expansion—contraction part of the cavity microchannel. The flow direction is from top to bottom in all images. The highlighted dimension, L_{ν} , on the image in the top row indicates how the length of the vortex is measured.

surfactant. The vortex lengths in these two solutions almost coincide at the same *Re* values for the range tested. The experimental data (excluding those after the vortices already reach the contraction walls, where the normalized vortex length becomes equal to unity in Fig. 4) can be fitted with a linear function as shown on the chart, which is consistent with our recent results of inertial expansion flow of water

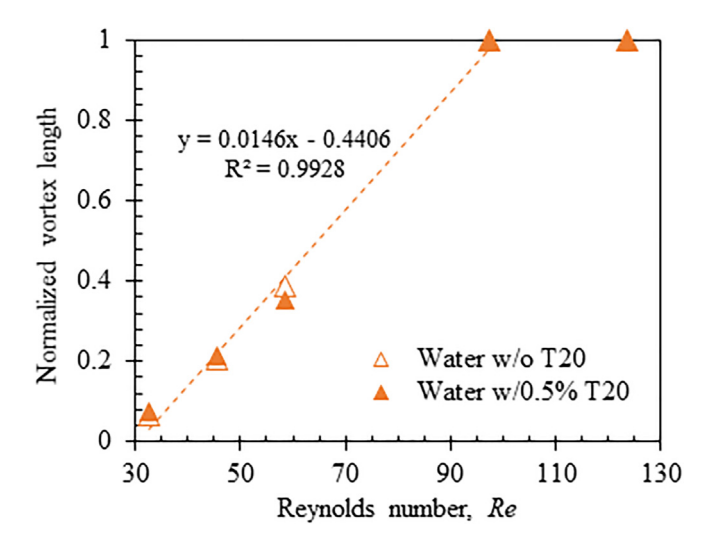


FIG. 4. Normalized (by the length of the cavity) vortex length (see L_V highlighted in Fig. 3) against the Reynolds number in the expansion flow of water with and without the addition of 0.5% Tween 20. The dashed line shows the linear trendline (the equation and R-squared value are both highlighted on the chart) for the average of the measured vortex lengths in the two solutions.

through both expansion–contraction 60 and contraction–expansion microchannels. 61 This observation indicates that the addition of Tween 20 at the concentration of $\mathcal{O}(0.1\% \text{ v/v})$ does not induce any visible elasticity or shear-thinning (see the viscosity profile in Fig. 2) effect into the inertial water flow.

B. Viscoelastic PEO solution

Similar to water, PEO solution has a (nearly) constant viscosity that is not altered by the addition of Tween 20 as shown in the viscosity curve in Fig. 2. It, however, has a mild elasticity, leading to significantly different flow patterns from water (see Fig. 3). Figure 5 shows the snapshots of cavity flow of PEO solutions with and without Tween 20. A range of flow rates from 1 to 40 ml/h was tested for which several events have been identified. However, for the two PEO solutions, all the events occur at the same Re values yet again, akin to the result of the inertial water flow (see Fig. 4). Specifically, the flow remains laminar and no viscoelastic disturbances occur at small flow rates. As the flow rate reaches 5 ml/h (Re = 19.5 and Wi = 37.0), the streamlines start to diverge and bend near the reentrant corners of the contraction walls. They get further disturbed and start overlapping each other at 10 ml/h (Re = 39.0 and Wi = 74.1) in the contraction flow. Concurrently, an unsteady flow is initiated near the salient corner of the expansion walls. It then interacts with the increasingly diverging and bending streamlines in the expansion flow leading to a chaotic flow over the entire cavity at 20 ml/h (Re = 78.0 and Wi = 148.1) and above.

The observed events for the cavity flow of PEO solutions in Fig. 5 are summarized in Fig. 6 with respect to the Weissenberg number. The same flow regimes are viewed at the same values of *Wi* (and hence *Re* for the Boger PEO solutions) in both the contraction and expansion

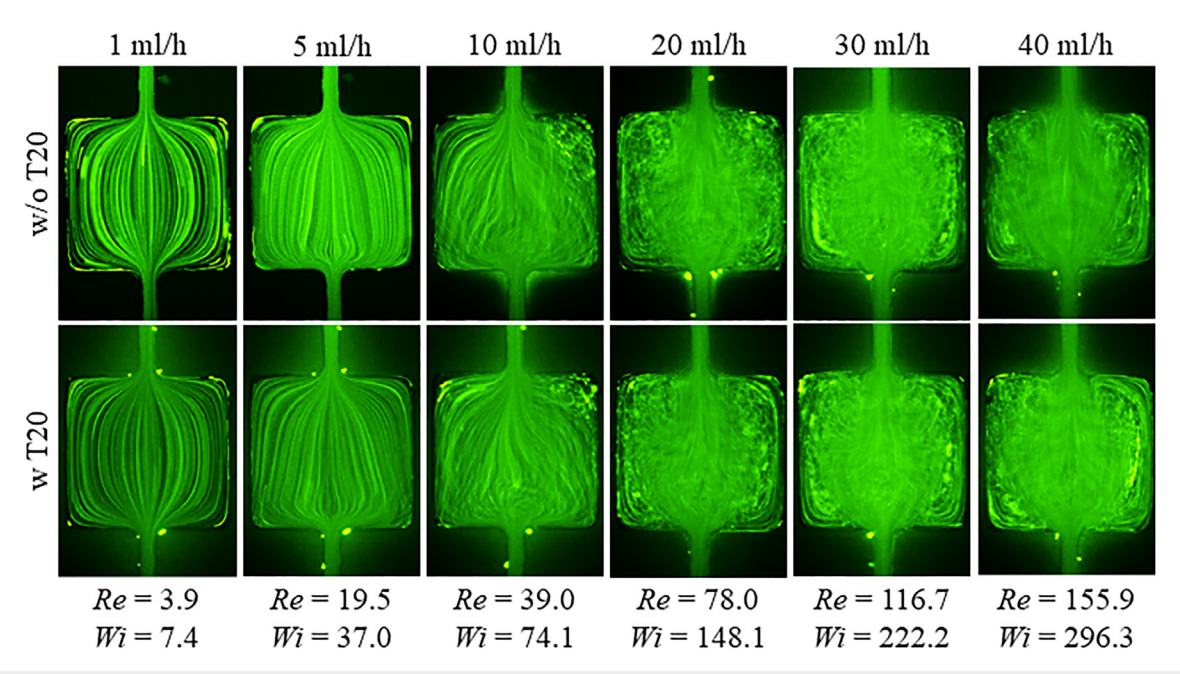


FIG. 5. Snapshot images of the flow of viscoelastic PEO solutions without (w/o T20, top row) and with (w T20, bottom row) 0.5% Tween 20 through the cavity microchannel. The flow direction is from top to bottom in all images.

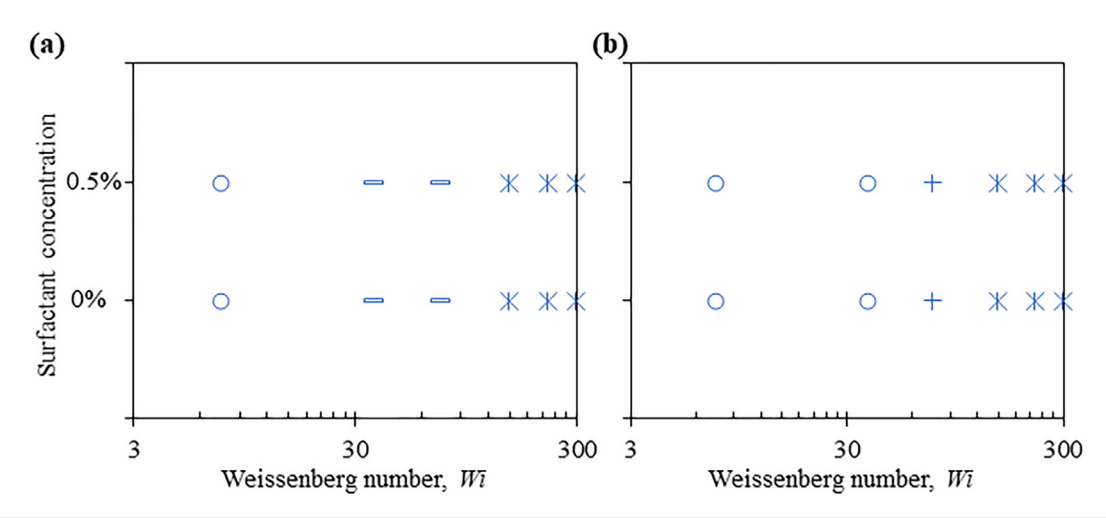


FIG. 6. Summary of the flow regimes with respect to the Weissenberg number for the contraction (a) and expansion (b) flows of PEO solutions with (0.5%) and without (0%) Tween 20 in the cavity microchannel: circles for no flow disturbances, rectangles for diverging/bending streamlines, pluses for unstable asymmetric vortices, and asterisks for chaotic flow.

flows with and without surfactant. This result, along with that for water (see Figs. 3 and 4), may be sufficient for us to make the hypothesis that the addition of Tween 20 at the concentration of $\mathcal{O}(0.1\% \text{ v/v})$ does not alter the fluid elasticity. Another explanation for the observed insignificant surfactant effect on the PEO solution lies in the neutral charge of the PEO polymer, ⁶² whose conformation is presumably not affected by the addition of small amount of neutral surfactant polymer like Tween 20. This explanation applies to the nonionic PAA solution ⁶³ as well, which will be presented later in Sec. III D.

C. Shear-thinning XG solution

Figure 7 shows the flow development of the XG solutions with and without Tween 20 in the cavity microchannel. The addition of Tween 20 reduces not only the fluid viscosity but also the shear thinning effect of the XG solution (see Fig. 2). However, both solutions still remain highly shear thinning as viewed from the values of the power-law index, n, in Table I. For the surfactant-free XG flow, stable symmetric corner vortices are formed in the contraction flow at the flow rate of $0.1 \,\mathrm{ml/h}$ (Re = 0.11) because of the strong shear thinning

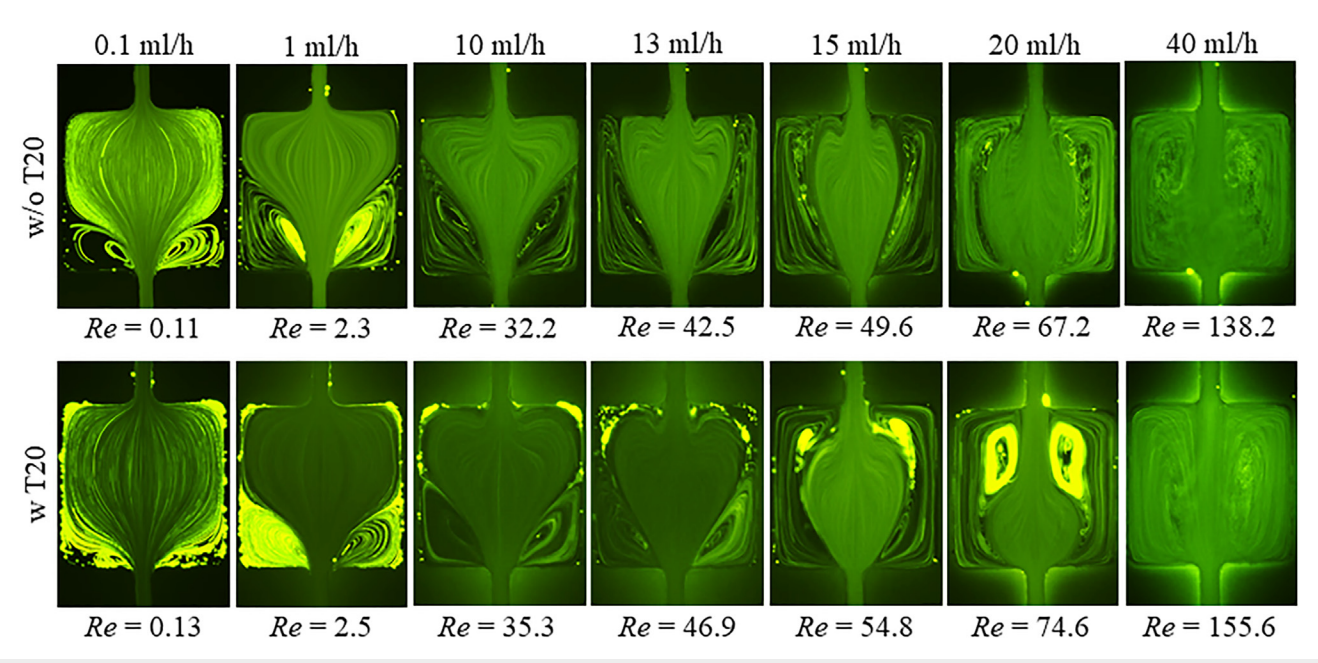


FIG. 7. Snapshot images of the flow of shear-thinning XG solution without (w/o T20, top row) and with (w T20, bottom row) 0.5% Tween 20 through the cavity microchannel. The flow direction is from top to bottom in all images.

effect. 51,60 They grow with the increase in the flow rate and extend till the expansion walls at 13 ml/h (Re = 42.6). Meanwhile, streamlines start bending in the expansion flow at 10 ml/h (Re = 32.2) because of the inertial effect. They develop into stable symmetric lip vortices at 13 ml/h, whose size is smaller than in the water flow at a similar Reynolds number. This is because the fluid shear thinning effect has been reported to stabilize the inertial expansion flow vortices. 51,53,60 At 15 ml/h (Re = 49.6), the expansion and contraction flow vortices start interacting with each other, such that the flow in the cavity becomes asymmetric and unstable for higher flow rates.

In contrast, the contraction flow vortices in the surfactant-added XG solution appear to be smaller at the same flow rates (for which the values of Re are also approximately equal) as in the surfactant-free solution because of the weaker shear thinning effect in the former. However, these vortices start interacting with the fluid inertia-induced expansion flow vortices at 13 ml/h (Re = 46.9) even before they extend till the expansion walls. This observation is different from that of the surfactant-free XG solution because the inertial expansion flow vortices are suppressed less by the less shear-thinning XG solution with surfactant. The contraction and expansion flow vortices merge together at 15 ml/h (Re = 54.8), which then develop into a pattern like that in the inertial water flow (Fig. 2) with the further increase in the flow rate. This phenomenon indicates the dominant inertial effect over the shear thinning effect in the XG solution with surfactant, particularly in the high Re regime. As XG is an anionic polymer,⁶⁴ its chains can interact with the neutrally charged Tween 20 polymer leading to changes in the morphology. Moreover, the screening of its charges by the surfactant polymers can possibly induce some flexibility and hence enhanced elasticity in the XG chains. However, the fluid elasticity effect, which should break the symmetry and draw instabilities into the cavity flow like the PEO solution does in Fig. 5, is not

observed in the XG solution with surfactant. This justifies our earlier hypothesis that the addition of surfactant at the concentration of $\mathcal{O}(0.1\% \text{ v/v})$ does not change the fluid elasticity.

Figure 8 compares the measured vortex lengths in the XG solutions with and without Tween 20. The surfactant-added XG solution displays smaller vortices in the contraction flow while larger vortices in the expansion flow, which can be explained by the reduced shear thinning effect as compared to the surfactant-free XG solution. The contraction flow vortex length follows a logarithmic dependence on Re in both XG solutions for Re of up to 30, where the effect of fluid inertia occurs. This trend is consistent with the observation in our recent study of surfactant-free XG flow in contraction-expansion microchannels, which highlights the role of the fluid shear thinning effect.⁵ Moreover, the expansion flow vortex length exhibits a linear trendline with respect to Re in only the XG solution with surfactant, which matches the observation of inertial-like cavity flow in the high Re regime as noted above. Figure 9 demonstrates the flow events for the two XG solutions in terms of Re. The initiation point for the flow instability clearly shifts to the higher Re in the XG solution with surfactant for both the contraction and expansion flows. This trend indicates the stabilizing effect of the addition of surfactant into the inelastic shear-thinning XG solution.

D. Viscoelastic and shear-thinning PAA solution

Figure 10 shows the snapshot images of the cavity flow of viscoelastic and shear thinning PAA solutions with and without Tween 20, respectively. The addition of surfactant causes a much larger decrease in both the viscosity and the shear-thinning effect (in terms of the power-law index, n, in Table I) of the PAA solution than those of the XG solution (see Fig. 2). For the surfactant-free PAA solution, which is more shear thinning than the surfactant-free XG solution, full-size

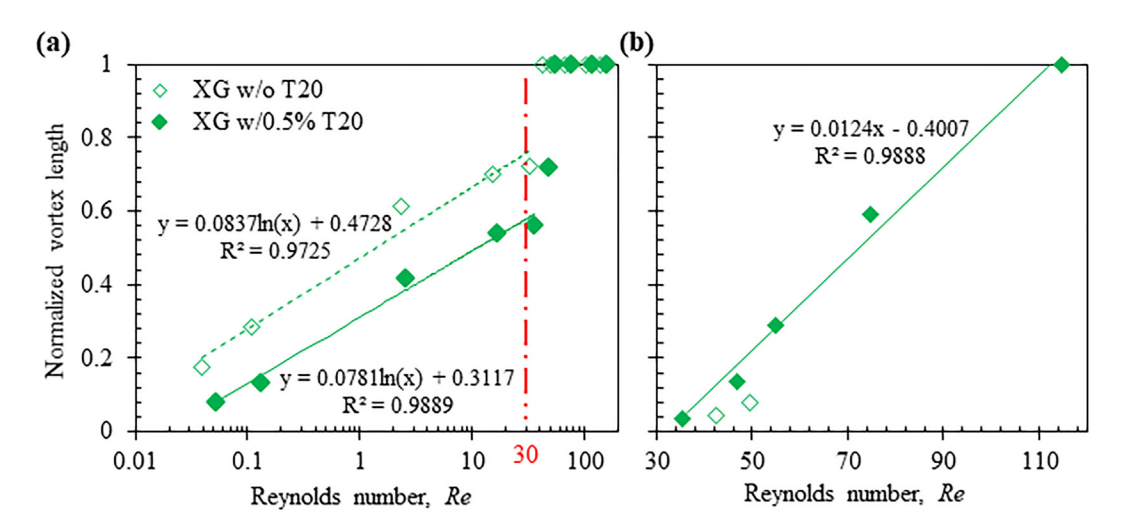


FIG. 8. Normalized (by the length of the cavity) vortex length against the Reynolds number in the contraction (a) and expansion (b) flows of XG solution with and without the addition of 0.5% Tween 20. The solid and dashed lines show the trendlines (the equation and R-squared value are both highlighted on the chart) for the measured vortex lengths in the surfactant-added and surfactant-free solutions, respectively. The vertical dashed-dotted line in (a) marks the transition to the flow regime where the fluid inertia takes effects.

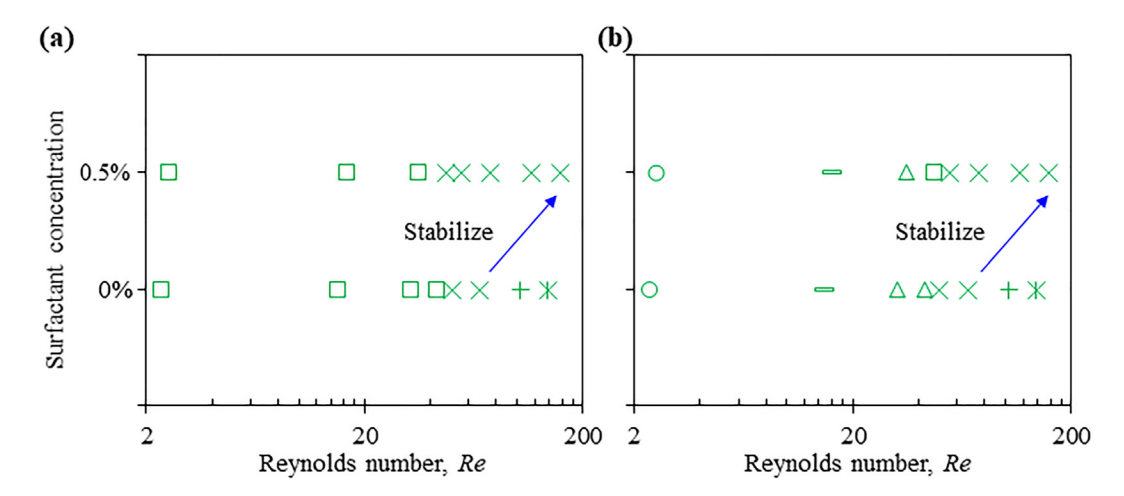


FIG. 9. Summary of the flow regimes in terms of the Reynolds number for the contraction (a) and expansion (b) flows of XG solution solutions with (0.5%) and without (0%) Tween 20 in the cavity microchannel: circles for no flow disturbances, rectangles for diverging/bending streamlines, triangles for stable lip vortices, squares for stable corner vortices, crosses for stable interaction of the contraction and expansion flow vortices, pluses for asymmetric and unstable vortices, and asterisks for chaotic flow.

corner vortices (i.e., the vortex length gets equal to the length of the cavity) are already formed in the contraction flow at $0.1 \,\mathrm{ml/h}$ (Re = 0.23, Wi = 46.9). These vortices become asymmetric at around 1 ml/h (Re = 3.1) as flow fluctuations occur inside the vortices. They also exhibit unstable oscillations with the increase in the flow rate to $10 \,\mathrm{ml}$ (Re = 33.8), at which no sign of inertial expansion flow vortices is observed. For flow rates of $13 \,\mathrm{ml/h}$ (Re = 44.0, Wi = 6098.8) and beyond, the cavity flow becomes completely chaotic.

The PAA solution with Tween 20 is a mildly shear thinning fluid with n = 0.72, as compared to the strongly shear thinning surfactant-free solution with n = 0.30. Consequently, the contraction flow vortices are completely absent in the surfactant-added PAA solution at the flow rate of 0.1 ml/h (Re = 0.38, Wi = 46.9). With the increasing

flow rate, lip vortices start to appear that grow on as steady large symmetric corner vortices till 5 ml/h (Re=23.5). They further extend till the expansion walls at 10 ml/h (Re=48.0), for which the inertial lip vortices are also observed on the expansion walls. The cavity flow to this point still remains stable with a symmetric pattern, unlike in the case of the surfactant free PAA solution. At 13 ml/h (Re=62.8), the contraction and expansion flows strongly interact, wherein the vortices become asymmetric and unstable. A completely chaotic flow is observed in the cavity at 20 ml/h (Re=97.7, Wi=9382.7) and beyond.

Figure 11 shows the plot for the measured vortex length vs *Re* in the cavity flow of PAA solution with and without Tween 20. The addition of surfactant reduces the contraction flow vortex size until the

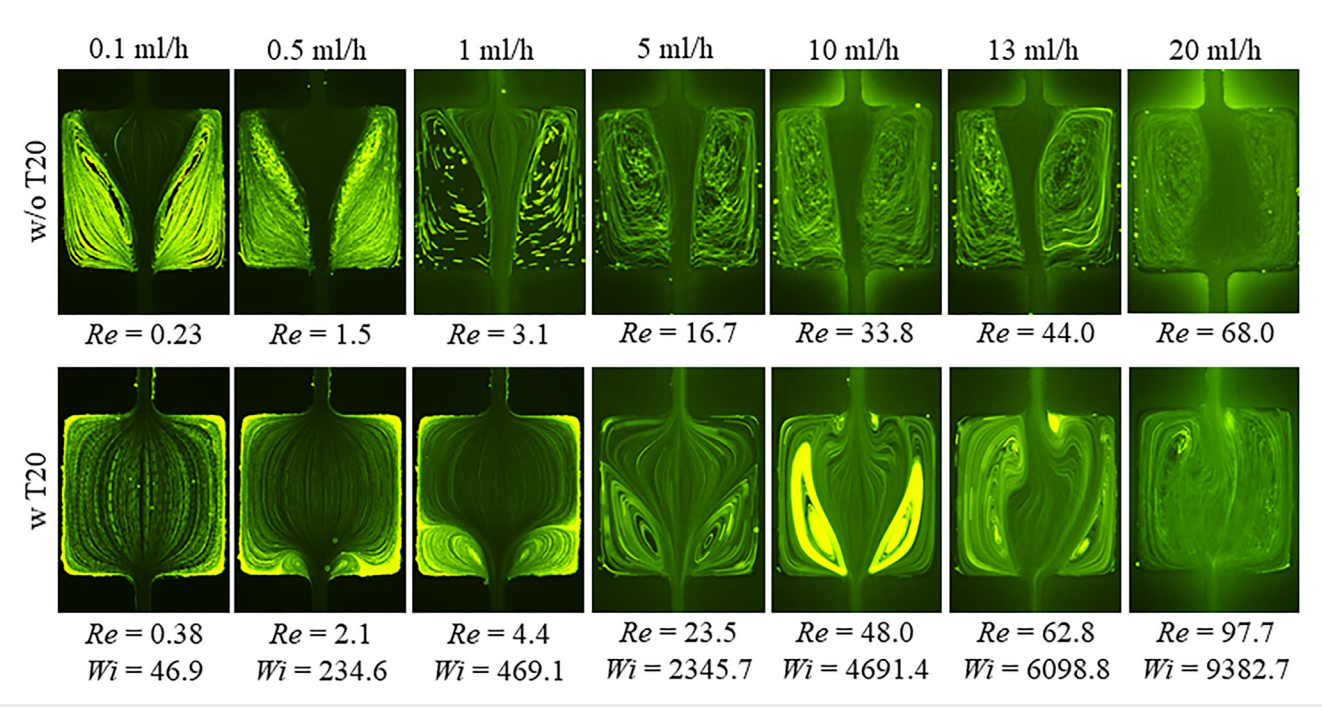


FIG. 10. Snapshot images of the flow of both viscoelastic and shear-thinning PAA solution without (w/o T20, top row) and with (w T20, bottom row) 0.5% Tween 20 through the cavity microchannel. The flow direction is from top to bottom in all images. Note that the *Wi* value in each column remains the same for the two images.

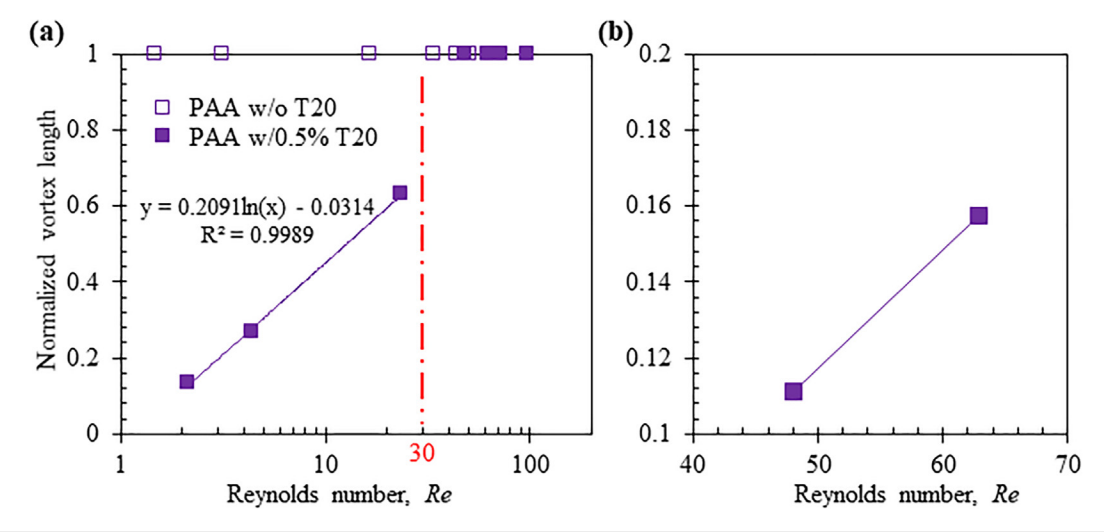


FIG. 11. Normalized (by the length of the cavity) vortex length against the Reynolds number in the contraction (a) and expansion (b) flows of PAA solution with and without the addition of 0.5% Tween 20. The solid line in (a) shows the trendline (the equation and R-squared value are both highlighted on the chart) for the measured contraction flow vortex length and the solid line (b) is used to guide the eyes only, both for the PAA solution with surfactant. The vertical dashed-dotted line in (a) marks the transition to the flow regime where the fluid inertia takes effects.

fluid inertial becomes prominent at around Re = 30 [see the vertical dashed-dotted line on the plot in (a) of Fig. 11], above which the vortex length becomes equal to the length of the cavity. It also induces the expansion flow vortices that are absent from the surfactant-free PAA

solution. Moreover, the contraction flow vortex length in the PAA solution with surfactant follows a logarithmic dependence on Re, so does the surfactant-free PAA solution for Re < 1 (data not included in Figs. 10 or 11). O All these observations are consistent with those for

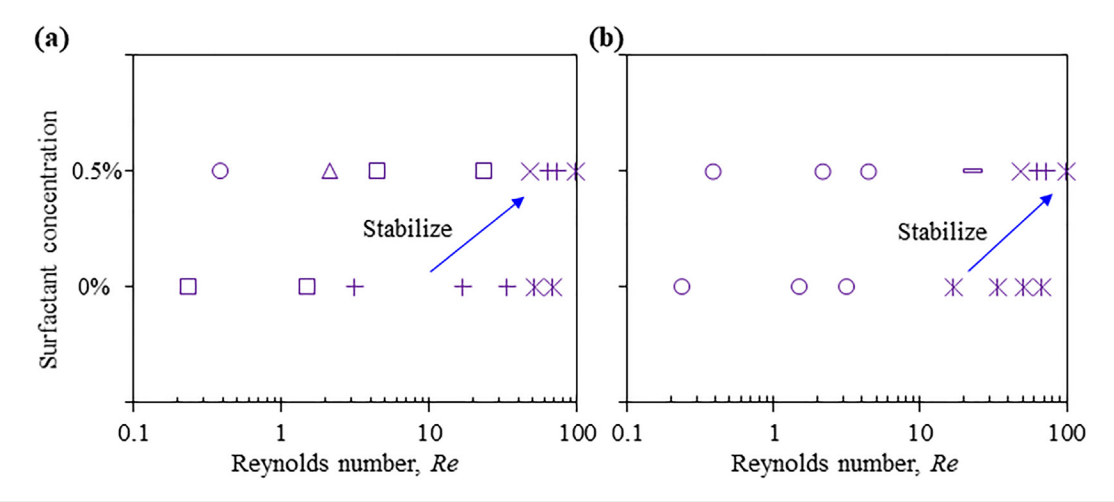


FIG. 12. Summary of the flow regimes in terms of the Reynolds number for the contraction (a) and expansion (b) flows of PAA solution solutions with (0.5%) and without (0%) Tween 20 in the cavity microchannel: circles for no flow disturbances, rectangles for diverging/bending streamlines, triangles for stable lip vortices, squares for stable corner vortices, crosses for stable interaction of the contraction and expansion flow vortices, pluses for asymmetric and unstable vortices, and asterisks for chaotic flow.

the two XG solutions, which should be a result of the fluid shear thinning effect. Figure 12 shows a summary of the flow regimes with respect to *Re* (instead of *Wi* for the purpose of direct comparison with Fig. 9 for the XG solutions) in the two PAA solutions. A similar stabilizing effect to the XG solutions is viewed for both the contraction and expansion flows. However, the flow regimes developed in the PAA solutions are different from those in the XG solutions because of the additional contribution of the strong fluid elasticity effect in the former.

IV. CONCLUSIONS

We have performed an experimental study of the effect of surfactant addition on the extensional flows of Newtonian water and non-Newtonian PEO, XG and PAA solutions in a single expansion-contraction microchannel. We find that the addition of 0.5% v/v Tween 20 causes a negligible change in the viscosity of water or PEO solution over a wide range of shear rates. It also has no significant impact on the flow pattern of either of the two originally constantviscosity fluids for Re of up to 200. These observations imply that the addition of 0.5% Tween 20 brings no additional elasticity to the fluid. However, such a surfactant addition causes a significant decrease in both the shear viscosity and the shear-thinning behavior of the XG and PAA solutions which both exhibit strong shear thinning effects. Moreover, it appears to increase the onset of flow instability to a higher Re and stabilize the cavity flow of both solutions. Our results indicate that Tween 20 surfactant favors fluids with shear thinning effects, which may be utilized to tune the flow behavior and even the particle migration therein. We will leave this for future work, where PEO solutions with different polymer concentrations and molecular weights^{65,6} can be used to obtain varying fluid elasticity and shear-thinning for a systematic study of surfactant effects. We will attempt to use pressure sensors to obtain the pressure drop across the contraction/expansion structure. We will also attempt to obtain the fluid extensional rheology and relate them to the pressure drop data for an improved understanding of the effect of surfactant addition on extensional flow. In addition, we admit that the current work lacks a quantitative analysis, which hopefully can be tackled through future collaborations.

ACKNOWLEDGMENTS

This work was supported in part by Clemson University through the Departmental Honors Undergraduate Research Program and Creative Inquiry Program (X.X.), China Scholarship Council (CSC)—Chinese Government Graduate Student Overseas Study Program (S.W.), University 111 Project of China under Grant No. B08046 (Y.S.), and NSF under Grant No. CBET-1750208 (J.B.B.).

AUTHOR DECLARATIONS

Conflict of Interest

The authors have no conflicts of interest to disclose.

AUTHOR CONTRIBUTIONS

M.D. and M.K.R. contributed equally to this work.

DATA AVAILABILITY

The data that support the findings of this study are available from the corresponding authors upon reasonable request.

REFERENCES

¹C. Barbati, J. Desroches, A. Robisson, and G. H. McKinley, "Complex fluids and hydraulic fracturing," Annu. Rev. Chem. Biomol. Eng. 7, 415–453 (2016).

²F. A. Mohsenatabar and H. R. Saghafi, "Review on chemical enhanced oil recovery using polymer flooding: Fundamentals, experimental and numerical simulation," Petroleum 6, 115–122 (2020).

³T. F. R. Alves, M. Morsink, F. Batain, M. V. Chaud, T. Almeida, D. A. Fernandes, C. F. da Silva, E. B. Souto, and P. Severino, "Applications of natural, semi-synthetic, and synthetic polymers in cosmetic formulations," Cosmetics 7, 75 (2020).

⁴H. Manikantan and T. M. Squires, "Surfactant dynamics: Hidden variables controlling fluid flows," J. Fluid Mech. 892, P1 (2020).

5N. Kumar and A. Mandal, "Surfactant stabilized oil-in-water nanoemulsion: Stability, interfacial tension, and rheology study for enhanced oil recovery application," Energy Fuels 32, 6452–6466 (2018).

- 6S. Mashaghi, A. Abbaspourrad, D. A. Weitz, and A. M. van Oijen, "Droplet microfluidics: A tool for biology, chemistry and nanotechnology," TrAC, Trends Anal. Chem. 82, 118–125 (2016).
- 7S. Sohrabi, N. Kassir, and M. M. Keshavarz, "Droplet microfluidics: Fundamentals and its advanced applications," RSC Adv. 10, 27560–27574 (2020).
- ⁸J. C. Baret, "Surfactants in droplet-based microfluidics," Lab Chip **12**, 422–433 (2012).
- ⁹K. J. Humphry, M. Kulkarni, D. A. Weitz, J. F. Morris, and H. A. Stone, "Axial and lateral particle ordering in finite Reynolds number channel flows," Phys. Fluids 22, 081703 (2010).
- ¹⁰J. M. Martel and M. Toner, "Inertial focusing dynamics in spiral microchannels," Phys. Fluids 24, 032001 (2012).
- ¹¹C. Liu, G. Hu, X. Jiang, and J. Sun, "Inertial focusing of spherical particles in rectangular microchannels over a wide range of Reynolds numbers," Lab Chip 15, 1168–1177 (2015).
- ¹²X. Wang, M. Zandi, C.-C. Ho, N. Kavalc, and I. Papautsky, "Single stream inertial focusing in a straight microchannel," Lab Chip. 15, 1812–1821 (2015).
- ¹³B. Kim, S. S. Lee, T. H. Yoo, and J. M. Kim, "Viscoelastic particle focusing in human bio fluids," Electrophoresis 42, 2238–2245 (2021).
- ¹⁴N. Xiang, Z. Ni, and H. Yi, "Concentration-controlled particle focusing in spiral elasto-inertial microfluidic devices," Electrophoresis 39, 417–424 (2018).
- ¹⁵D. Yuan, S. Yadav, H. T. Ta, H. Fallahi, H. An, N. Kashaninejad, C. H. Ooi, N.-T. Nguyen, and J. Zhang, "Investigation of viscoelastic focusing of particles and cells in a zigzag microchannel," Electrophoresis 42, 2230–2237 (2021).
- 16D. Li, X. Shao, J. B. Bostwick, and X. Xuan, "Particle separation in xanthan gum solutions," Microfluid. Nanofluid. 23, 125 (2019).
- gum solutions," Microfluid. Nanofluid. 23, 125 (2019).

 17 E. J. Lim, T. J. Ober, J. F. Edd, S. P. Desai, D. Neal, K. W. Bong, P. S. Doyle, G. H. McKinley, and M. Toner, "Inertio-elastic focusing of bioparticles in microchannels at high throughput," Nat. Commun. 5, 4120 (2014).
- ¹⁸R. Del Sorbo, S. Prévost, E. Schneck, M. Gradzielski, and I. Hoffmann, "On the mechanism of shear-thinning in viscous oppositely charged polyelectrolyte surfactant complexes (PESCs)," J. Phys. Chem. B 124, 909–913 (2020).
- ¹⁹F. Ye, W. Zhu, W. Jiang, Z. Wang, Q. Chen, X. Gong, and S. Xuan, "Influence of surfactants on shear-thickening behavior in concentrated polymer dispersions," J. Nanopart. Res. 15, 2122 (2013).
- ²⁰P. K. Bollineni, G. Dordzie, S. O. Olayiwola, and M. Dejam, "An experimental investigation of the viscosity behavior of solutions of nanoparticles, surfactants, and electrolytes," Phys. Fluids 33, 026601 (2021).
- ²¹J. Xu, P. Dong, H. Zhao, C. P. Tostado, and G. S. Luo, "The dynamic effects of surfactants on droplet formation in coaxial microfluidic devices," Langmuir 28, 9250–9258 (2012).
- ²²J. Yang and R. Pal, "Investigation of surfactant-polymer interactions using rheology and surface tension measurements," Polymers 12, 2302 (2020).
- ²³C. D. V. Martínez Narváez, T. Mazur, and V. Sharma, "Dynamics and extensional rheology of polymer-surfactant association complexes," Soft Matter 17, 6116–6126 (2021).
- ²⁴S. Ahmadikhamsi, F. Golfier, C. Oltean, E. Lefèvre, and S. A. Bahrani, "Impact of surfactant addition on non-Newtonian fluid behavior during viscous fingering in Hele–Shaw cell," Phys. Fluids 32, 012103 (2020).
- ²⁵G. D'Avino, F. Greco, and P. L. Maffettone, "Particle migration due to viscoelasticity of the suspending liquid and its relevance in microfluidic devices," Annu. Rev. Fluid Mech. 49, 341–360 (2017).
- ²⁶C. Liu and G. Hu, "High-throughput particle manipulation based on hydrodynamic effects in microchannels," Micromachines 8, 73 (2017).
- ²⁷X. Lu, C. Liu, G. Hu, and X. Xuan, "Particle manipulations in non-Newtonian microfluidics: A review," J. Colloid Interface Sci. 500, 182–201 (2017).
- ²⁸F. Tian, Q. Feng, Q. Chen, C. Liu, T. Li, and J. Sun, "Manipulation of biomicro/nanoparticles in non-Newtonian microflows," <u>Microfluid. Nanofluid.</u> 23, 68 (2019).
- ²⁹J. Zhou and I. Papautsky, "Viscoelastic microfluidics: Progress and challenges," Microsys. Nanoeng. 6, 113 (2020).
- 30S. J. Haward, J. Page, T. A. Zaki, and A. Q. Shen, "Phase diagram for viscoelas—tic Poiseuille flow over a wavy surface," Phys. Fluids 30, 113101 (2018).
- ³¹Q. Zhao, D. Yuan, J. Zhang, and W. Li, "A review of secondary flow in inertial microfluidics," Micromachines 11, 461 (2020).

- ³²R. Tao, T. Ng, Y. Su, and Z. Li, "A microfluidic rectifier for Newtonian fluids using asymmetric converging–diverging microchannels," Phys. Fluids 32, 052010 (2020).
- ³³D. Jiang, C. Ni, W. Tang, D. Huang, and N. Xiang, "Inertial microfluidics in contraction–expansion microchannels: A review," Biomicrofluidics 15, 041501 (2021).
- ³⁴E. Jafari Nodoushan, Y. J. Lee, G. Lee, and N. Kim, "Quasi-static secondary flow regions formed by microfluidic contraction flows of wormlike micellar solutions," Phys. Fluids 33, 093112 (2021).
- 35R.-J. Yang, H.-H. Hou, Y.-N. Wang, C.-H. Lin, and L.-M. Fu, "A hydrodynamic focusing microchannel based on micro-weir shear lift force," Biomicrofluidics 6, 034110 (2012).
- ³⁶J. Zhou, S. Kasper, and I. Papautsky, "Enhanced size-dependent trapping of particles using microvortices," Microfluid, Nanofluid, 15, 611–623 (2013).
- particles using microvortices," Microfluid. Nanofluid. 15, 611–623 (2013).

 37 R. Khojah, R. Stoutamore, and D. D. Carlo, "Size-tunable microvortex capture of rare cells," Lab Chip 17, 2542–2549 (2017).
- ⁵⁸F. Shen, S. Xue, M. Xu, Y. Pang, and Z. Liu, "Experimental study of single-particle trapping mechanisms into microcavities using microfluidics," Phys. Fluids 31, 042002 (2019).
- ³⁹F. Shen, Z. Li, M. Ai, H. Gao, and Z. Liu, "Round cavity-based vortex sorting of particles with enhanced holding capacity," Phys. Fluids 33, 082002 (2021).
- particles with enhanced holding capacity," Phys. Fluids 33, 082002 (2021).

 40S. Cha, K. Kang, J. B. You, S. G. Im, Y. Kim, and J. M. Kim, "Hoop stress-assisted three-dimensional particle focusing under viscoelastic flow," Rheol. Acta 53, 927–933 (2014).
- ⁴¹D. Yuan, J. Zhang, S. Yan, C. Pan, G. Alici, N. T. Nguyen, and W. Li, "Dean-flow-coupled elasto-inertial three-dimensional particle focusing under viscoelastic flow in a straight channel with asymmetrical expansion—contraction cavity arrays," Biomicrofluidics 9, 044108 (2015).
- ⁴²D. Yuan, J. Zhang, R. Sluyter, Q. Zhao, S. Yan, G. Alicia, and W. Li, "Continuous plasma extraction under viscoelastic fluid in a straight channel with asymmetrical expansion–contraction cavity arrays," Lab Chip 16, 3919–3928 (2016).
- ⁴³L. Fan, Z. Tian, J. Zhe, and L. Zhao, "Efficient microfluidic enrichment of nano-/submicroparticle in viscoelastic fluid," Electrophoresis 42, 2273–2280 (2021).
- ⁴⁴M. K. Raihan, D. Li, A. J. Kummetz, L. Song, L. Yu, and X. Xuan, "Vortex trapping and separation of particles in shear thinning fluids," Appl. Phys. Lett. 116, 183701 (2020).
- ⁴⁵R. Hidema, T. Oka, Y. Komoda, and H. Suzuki, "Effects of flexibility and entanglement of sodium hyaluronate in solutions on the entry flow in micro abrupt contraction—expansion channels," Phys. Fluids 31, 072005 (2019).
- ⁴⁶T. Tomkovic, E. Mitsoulis, and S. G. Hatzikiriakos, "Contraction flow of ionomers and their corresponding copolymers: Ionic and hydrogen bonding effects," Phys. Fluids 31, 033102 (2019).
- ⁴⁷C. Sasmal, "Flow of wormlike micellar solutions through a long micropore with step expansion and contraction," Phys. Fluids 32, 013103 (2020).
- ⁴⁸L. L. Ferrás, A. M. Afonso, M. A. Alves, J. M. Nóbrega, and F. T. Pinho, "Newtonian and viscoelastic fluid flows through an abrupt 1:4 expansion with slip boundary conditions," Phys. Fluids 32, 043103 (2020).
- ⁴⁹P. R. Varges, B. S. Fonseca, P. R. de Souza Mendes, M. F. Naccache, and C. R. de Miranda, "Flow of yield stress materials through annular abrupt expansion—contractions," Phys. Fluids 32, 083101 (2020).
- 50J. Musil and M. Zatloukal, "Flow-induced birefringence study of secondary flow in entrance region of rectangular slit channel for long-chain branched polyethylene melt," Phys. Fluids 34, 013103 (2022).
- ⁵¹P. P. Jagdale, D. Li, X. Shao, J. B. Bostwick, and X. Xuan, "Fluid rheological effects on the flow of polymer solutions in a contraction–expansion microchannel," Micromachines 11, 278 (2020).
- 52D. F. James, "Boger fluids," Annu. Rev. Fluid Mech. 41, 129–142 (2009).
- ⁵³M. K. Raihan, S. Wu, Y. Song, and X. Xuan, "Constriction length dependent instabilities in the microfluidic entry flow of polymer solutions," Soft Matter 17, 9198–9209 (2021).
- 54I. Wong and C.-M. Ho, "Surface molecular property modifications for poly (dimethylsiloxane) (PDMS) based microfluidic devices," Microfluid. Nanofluid. 7, 291–306 (2009).
- 55R. B. Bird, R. C. Armstrong, and O. Hassager, Dynamics of Polymeric Liquids (Wiley-Interscience, Hoboken, 1987), Vol. 1.

- ⁵⁶S. Haase, J. A. Wood, L. M. J. Sprakel, and R. G. H. Lammertink, "Inelastic non-Newtonian flow over heterogeneously slippery surfaces," Phys. Rev. E 95, 023105 (2017).
- ⁵⁷L. E. Rodd, T. P. Scott, D. V. Boger, J. J. Cooper-White, and G. H. McKinley, "The inertioelastic planar entry flow of low-viscosity elastic fluids in micro-fabricated geometries," J. Non-Newtonian Fluid Mech. 129, 1–22 (2005).
- ⁵⁸R. J. Poole and M. P. Escudier, "Turbulent flow of viscoelastic liquids through an axisymmetric sudden expansion," J. Non-Newtonian Fluid Mech. 117, 25–46 (2004).
- ⁵⁹A. Lindner, D. Bonn, and J. Meunier, "Viscous fingering in a shear-thinning fluid," Phys. Fluids 12, 256–261 (2000).
- ⁶⁰M. K. Raihan, P. P. Jagdale, S. Wu, X. Shao, J. B. Bostwick, X. Pan, and X. Xuan, "Flow of non-Newtonian fluids in a single-cavity microchannel," Micromachines 12, 836 (2021).

- ⁶¹D. Li, L. Song, C. Zhang, L. Yu, and X. Xuan, "A depth-averaged model for Newtonian fluid flows in shallow microchannels," Phys. Fluids 33, 012002 (2021).
- ⁶²J. Horvath and V. Dolník, "Polymer wall coatings for capillary electrophoresis," Electrophoresis 22, 644–655 (2001).
- ⁶³E. Pefferkorn, "Polyacrylamide at solid/liquid interfaces," J. Colloid Interface Sci. 216, 197–220 (1999).
- ⁶⁴J. Patel, B. Maji, N. S. H. Narayana Moorthy, and S. Maiti, "Xanthan gum derivatives: Review of synthesis, properties and diverse applications," RSC Adv. 10, 27103–27136 (2020).
- 65S. Wu, M. K. Raihan, L. Song, X. Shao, J. B. Bostwick, L. Yu, X. Pan, and X. Xuan, "Polymer effects on viscoelastic fluid flows in a planar constriction microchannel," J. Non-Newtonian Fluid Mech. 290, 104508 (2021).
- ⁶⁶C. Liu, B. Ding, C. Xue, Y. Tian, G. Hu, and J. Sun, "Sheathless focusing and separation of diverse nanoparticles in viscoelastic solutions with minimized shear thinning," Anal. Chem. 88, 12547–12553 (2016).